

Mio-Pliocene magnetostratigraphy in the southern Carpathian foredeep and Mediterranean–Paratethys correlations

Iuliana Vasiliev,^{1,2} Wout Krijgsman,¹ Marius Stoica³ and Cor G. Langereis¹

¹Paleomagnetic Laboratory 'Fort Hoofddijk', Faculty of Geosciences, Utrecht University, Budapestlaan 17, 3584 CD Utrecht, The Netherlands; ²Netherlands Centre for Integrated Solid Earth Sciences (ISES), Faculty of Geology and Geophysics, Bucharest University, Bălcescu Bd. 1, 010041, Romania; ³Department of Geology and Paleontology, Faculty of Geology and Geophysics, Bucharest University, Bălcescu Bd. 1, 010041, Romania

ABSTRACT

A full understanding of the Mio-Pliocene palaeogeographical and palaeoenvironmental changes in the circum-Mediterranean region during the Messinian Salinity Crisis (MSC) is at present hampered by the lack of reliable chronostratigraphic correlations between the Mediterranean and Paratethys regions. Here, we present magnetostratigraphic ages for the Upper Miocene to Pliocene deposits of the southern Carpathian foredeep in Romania. These ages are in good agreement with those recently obtained from the eastern Carpathian foredeep and define a new chronology for the eastern Paratethys. The Meotian/Pontian boundary is not biostratigraphically

constrained in our sections, but according to the geological map of the region arrives at ~5.8 Ma. The Pontian/Dacian boundary is dated at c. 4.8 Ma and the Dacian/Romanian boundary at c. 4.1 Ma. The main part of the MSC (5.96–5.33 Ma) is thus represented by the Pontian Stage, but the observed palaeoenvironmental and biostratigraphic changes in our sections of the eastern Paratethys do not indicate any relation with the dramatic desiccation and reflooding events of the Mediterranean.

Terra Nova, 17, 376–384, 2005

Introduction

Magnetostratigraphy and correlation to the geomagnetic polarity time scale (GPTS) has become a standard tool in earth sciences, especially because it can be applied to a wide variety of rock types and in different (marine/continental) environments. There are several prerequisites for a successful application of magnetostratigraphy as a dating technique for sedimentary rocks. A suitable sedimentary sequence has to be continuous, without major hiatuses or changes in sedimentation rate and must represent a long enough period of time to reveal the characteristic pattern of reversals. In addition, some approximate age control should be available from biostratigraphy or radiometric dating. Once these prerequisites have been met, magnetostratigraphy can be used to obtain reliable and accurate time constraints on the age and duration of geodynamic and palaeoclimatological events.

In the Mediterranean region, a reliable magnetostratigraphic time frame has been developed for the late Miocene marine and continental sequences that straddle the Messinian Salinity Crisis (MSC) (Gautier *et al.*, 1994; Garcés *et al.*, 2001). This time scale is essential to understand the faunal and floral responses of a progressively desiccating Mediterranean Sea (Suc and Bessais, 1990; Benammi *et al.*, 1996; Garcés *et al.*, 1998) and it supported the conclusion that tectonic processes had been more important than glacio-eustatic processes during the isolation of the Mediterranean (Hodell *et al.*, 2001; Krijgsman *et al.*, 2004). The latest (Lago Mare) phase of the MSC is characterized by the dominance of caspo-brackish fauna (mainly ostracods), of Paratethyan affinities (Cita *et al.*, 1978, 1990).

To fully comprehend the circum-Mediterranean palaeogeographical evolution, it is important that the Paratethys sequences can be correlated in detail to the Mediterranean sequences. However, a reliable time scale for the Miocene–Pliocene sedimentary record of the Paratethys is still lacking. Radiometric datings are scarce and biochronology is hampered by the dominance of regional endemic species. Reliable magnetostratigraphic

studies are also virtually absent, despite the presence of suitable sequences. Consequently, chronostratigraphic control for the Paratethys is still very limited and the various time scales are ambiguously different (Semenenko, 1979; Alexeeva *et al.*, 1981; Andreescu, 1981; Steininger *et al.*, 1996). Recently, a high-resolution magnetostratigraphic record was constructed for the Meotian to Romanian (7.2–2.5 Ma) time interval in the eastern Carpathian foredeep (Vasiliev *et al.*, 2004). In this new time scale, the Pontian Stage comprises the interval between 5.8 Ma and 4.8 Ma. The main part of the Mediterranean MSC, which was dated to occur between 5.95 and 5.53 Ma (Krijgsman *et al.*, 1999), thus closely – but not exactly – correlates to the lower part of the Pontian in the eastern Paratethys.

In this paper, we present the magneto-biostratigraphic results of the Upper Miocene–Lower Pliocene sedimentary sequences of the southern Carpathian foredeep. We will test if the East Carpathian ages are valid for the entire foredeep, or that local palaeoenvironmental conditions are important. Our new chronology for the Carpathian foredeep of Romania furthermore allows a direct correlation to the marine and continental

Correspondence: I. Vasiliev, Paleomagnetic Laboratory 'Fort Hoofddijk', Utrecht University, Budapestlaan 17, 3584 CD Utrecht, The Netherlands. Tel.: +31.30.253.1361; fax: +31.30.253.1677; e-mail: vasiliev@geo.uu.nl

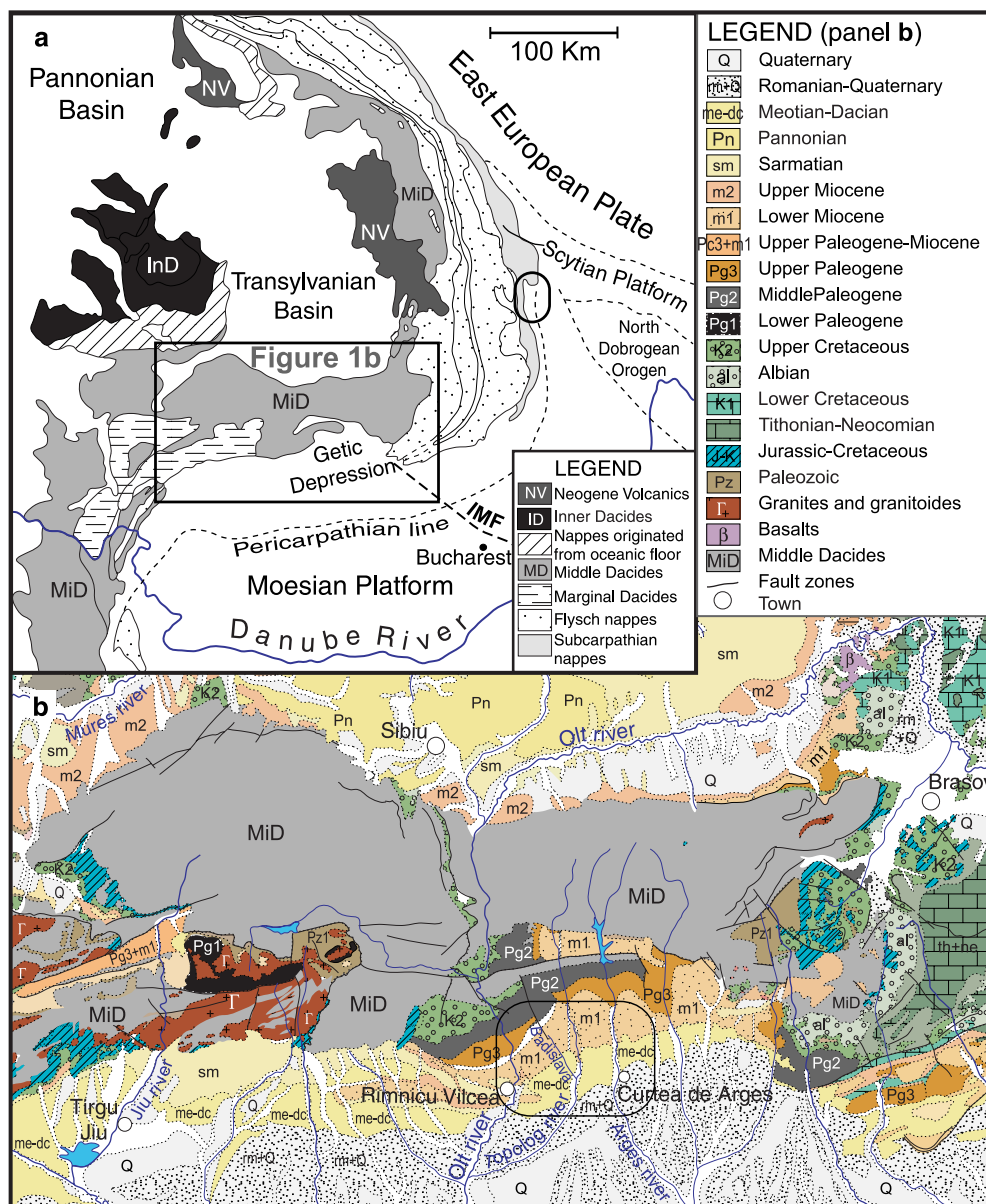


Fig. 1 Schematic geological map of the Romanian Carpathians (after Sandulescu, 1988) and the location of the Getic Depression. (a) The study area of Vasiliev *et al.* (2004) in the eastern Carpathians is indicated by the small oval. (b) Geological map of the study area in the southern Carpathian foredeep (after the geological map of Romania, 1978 at 1 : 1 000 000 scale).

sequences of the Mediterranean region.

Geological setting and sections

The different faunal evolution of the Neogene epicontinental seas, north and south of the Alpine–Caucasian orogenic belt, motivated Laskarev (1924) to subdivide the Tethys realm into a northern Paratethys bioprovince and a southern Mediterranean

bioprovince. In addition, the Paratethys itself was again subdivided into smaller basins and domains, the western Paratethys comprising the Pannonian and Transylvanian basins and the eastern Paratethys with the Dacian, Black Sea and Caspian basins (details in Alexeeva *et al.*, 1981; Andreescu, 1981; Steininger *et al.*, 1988, 1996; Semenenko, 1989; Rögl, 1996). The western and eastern Paratethys domains were separated by the Car-

pathian orogen, which was tectonically uplifted to become a barrier during the Middle Miocene.

In late Miocene (Sarmatian–Meotian) times, the palaeogeographical evolution of the Dacian Basin is closely related to the eastern Paratethys, but in Pliocene (Romanian–Dacian) times, it shows more affinities with the western Paratethys. Consequently, the geological time scales for the Dacian Basin are generally a

combination of western and eastern Paratethys time scales, resulting in major controversies, uncertainties and confusion.

We have selected the southern Carpathian foredeep, or Getic depression (Fig. 1), for a high-resolution integrated magneto-biostratigraphic study of the western Dacian Basin. The Getic depression represents the sedimentary basin that developed at the contact between the South Carpathian nappe pile and the Moesian Platform (Sandulescu, 1984). We sampled two long sedimentary sequences along the Bădăslava and Topolog rivers, which are located between the towns of Rîmnicu Vâlcea and Curtea de Argeş (Fig. 1b). A total number of 180 levels were cored in the 1092 m thick Bădăslava river section, while 62 levels were sampled in the 850 m thick Topolog section. All samples have been taken from riverbeds where the rock surfaces were freshly cleaned by the stream. The sedimentary sequence has a bedding dip between 15° and 20° to the south and consists of an alternation of blue to grey sandstones, siltstones and clays. Our sections start stratigraphically in deposits of upper Meotian deposits and end at lower Romanian sediments near the confluence of the Bădăslava and Topolog rivers. The sections thus comprise rocks of the Meotian, Pontian, Dacian and Romanian stages, which are very well exposed along the two river incisions. The upper Meotian part of the section is relatively coarse grained containing blue-grey sandy-silty units. The Pontian and lower Dacian are more fine grained consisting of bluish (silty) clays, while the upper Dacian and lower Romanian become progressively coarser again, showing many intercalations of organic-rich (lignite) layers as well.

Biostratigraphy

Extensive biostratigraphic studies have been performed in the southern Carpathian foredeep between the Olt and Argeş valleys (Fig. 1b), focusing mainly on mollusc and ostracod assemblages (Bombita *et al.*, 1967; Lazar, 1987). Detailed qualitative and quantitative analysis of the ostracod and mollusc species collected from this region allowed the establishment of characteristic assemblages for each

stage. The observed associations from the study area indicate the presence of Meotian, Pontian, Dacian and Romanian deposits. The geological maps of the southern Carpathian foredeep are largely based on these fossil assemblages.

In the Bădăslava and Topolog valleys, no fossil localities are reported in the sedimentary units that are lateral equivalents of the Meotian and lowermost Pontian; the Meotian/Pontian boundary is determined by geological mapping. In contrast,

Table 1 Ostracofauna and macrofauna from the region between Olt and Argeş valleys of the southern Carpathians

Ostracofauna	Macrofauna (molluscs)
(Sub) stage – DACIAN	
Lithology – marls, clays and sands	
	Bivalvia
<i>Cyprideis</i> sp.	<i>Hyriopsis</i> sp.
<i>Cytherissa lacustris</i>	<i>Zamphiridacna orientalis</i>
<i>Cytherissa bogatschovi</i>	<i>Prosodacna (Prosodacna) semisulcata</i>
<i>Heterocypris</i> sp.	<i>Prosodacna (Prosodacna) serrena</i>
<i>Leptocythere</i> sp.	<i>Dacicardium rumanum</i>
<i>Amnicythere palimpsesta</i>	<i>Charthoconcha bayerni</i>
<i>Loxococoncha ex gr. petasa</i>	<i>Stylodacna heberti</i>
<i>Scottia dacica</i>	<i>Dreissena rumana</i>
<i>Scottia ex gr. bonei</i>	<i>Dreissena rimestiensis</i>
<i>Scottia</i> sp.	<i>Dreissena polymorpha</i>
<i>Amplocypris dorosobrevis</i>	<i>Dreissena berbestiensis</i>
<i>Candona neglecta</i>	Gastropoda
<i>Candona (Caspioypris)</i> sp.	<i>Viviparus argesiensis</i>
<i>Candona (Pontoniella)</i> sp.	<i>Viviparus muscelensis</i>
<i>Candona (Caspioella) lobata</i>	<i>Viviparus duboisi</i>
<i>Candona (Caspioella) balcanica</i>	<i>Viviparus berbestiensis</i>
<i>Candona (Caspioella) ossoinae</i>	<i>Viviparus monasterialis</i>
	<i>Bulimus (Tylopoma) speciosus</i>
	<i>Lithoglyphus acutus decipiens</i>
(Sub) stage – PONTIAN	
Lithology – marly	
	Bivalvia
<i>Candona (Caspioypris) alta</i>	<i>Caladacna steindachneri</i>
<i>Candona (Pontoniella) acuminata striata</i>	<i>Limnocardium (Tauricardium) petersi nasyrica</i>
<i>Candona (Caspioypris)</i> sp.	<i>Limnocardium (Arpadicardium) peregrinum</i>
<i>Candona (Caspioella) balcanica</i>	<i>Lunadacna lunae</i>
<i>Candona (Caspioella) venusta</i>	<i>Pseudocatyclus</i> sp.
<i>Candona (Caspioella) lobata</i>	<i>Prosodacna (Prosodacna) semisulcata antiqua</i>
<i>Candona (Pontoniella) sp.</i>	<i>Prosodacna (Prosodacna) semisulcata angustata</i>
<i>Cypria tocorjescui</i>	<i>Limnocardium (Euxinocardium) sacelum</i>
<i>Bakunella dorsoarcuata</i>	Gastropoda
<i>Amnicythere palimpsesta</i>	<i>Valenciennius krambergeri</i>
<i>Leptocythere</i> sp.	<i>Valenciennius facetus rotundus</i>
<i>Candona (Caspioella) ossoinae</i>	
<i>Tyrrhenocythere filipescui</i>	
	Lithology – sandy
	Bivalvia
<i>Tyrrhenocythere filipescui</i>	<i>Dacicardium vetustum</i>
<i>Tyrrhenocythere motasi</i>	<i>Pontalmyra (Pontalmyra) dacica</i>
<i>Bakunella dorsoarcuata</i>	<i>Pontalmyra (Pontalmyra) concina</i>
<i>Amplocypris dorosobrevis</i>	<i>Pseudoprosodacna</i> sp.
<i>Amplocypris</i> sp.	<i>Prosodacnomya sturii sabbae</i>
<i>Candona (Caspioella) venusta</i>	<i>Hyriopsis</i> sp.
<i>Candona (Caspioella) lobata</i>	<i>Unio (Unio) sp.</i>
<i>Candona (Caspioella) ossoinae</i>	Gastropoda
<i>Candona (Caspioella) balcanica</i>	<i>Viviparus incertus</i>

Table 1 *Continued*

Ostracofauna	Macrofauna (molluscs)
<i>Candona (Caspiocypris) alta</i>	<i>Teodoxus</i> sp.
<i>Candona (Caspiocypris)</i> sp.	<i>Melanopsis decollata</i>
<i>Candona (Pontoniella)</i> sp.	
<i>Cypria tocorjescui</i>	
<i>Scottia</i> sp.1	
<i>Scottia</i> sp.2	
<i>Cyprideis</i> sp.	
<i>Loxoconcha petasa</i>	
<i>Amnicythère</i> sp.	

the upper Pontian and Dacian sedimentary rocks are very rich in well-preserved fossil assemblages. The characteristic ostracod and mollusc assemblages of the Pontian is subdivided between two distinct facies: (i) the sandy facies type characterized by the abundance of the ostracod species *Tyrrhenocythere filipescui* (HANGANU), *Tyrrhenocythere motasi* OLTEANU, *Amplocypris dorsobrevis* SOKAC and *Bakunella dorsoarcuata* (ZALÁNYI) and (ii) the marly facies characterized by the abundance of the *Cypria tocorjescui* HANGANU, *Candona (Pontoniella) acuminata striata* MANDELSTAM, *Candona (Caspiocypris) alta* (ZALÁNYI), *Amnicythère palimpsesta* (LIVENTAL) (Table 1). In the mollusc assemblages, the presence of *Lunadacna lunae* (VOITEST1) is a key element because its first occurrence characterizes the Upper Pontian (Bosphorinan substage). It is associated with *Caladacna steindachneri* BRUSINA, *Chartochoncha bayerni* (R. HOERNES), *Limnocardium (Tauricardium) petersi* nasyrica EBERSIN, *Valenciennius faceatus rotundus* TAKTASVILI and *V. krambergeri* R. HOERNES.

Index species for the Lower Dacian (Getian substage) are mainly represented by Cyprideis species, which are always accompanied by *Cytherissa lacustris* (SARS), *C. bogatschovi* (LIVENTAL), *Candona (Caspiolla) balcanica* (ZALÁNYI), *Heterocypris* sp., *Scottia dacica* HANGANU. The presence of *Zamphiridacna orientalis* (SABBA) (Table 1) is especially important because its first occurrence corresponds to the Pontian/Dacian boundary and is frequently associated with *Dacicardium rumanum* (FONTANNES) and *Pachydacna (Parapachydacna) serrena* (SABBA).

Palaeomagnetic results

Rock magnetic experiments

Several rock-magnetic experiments were performed to identify the carriers of the natural remanent magnetization (NRM). Thermomagnetic measurements (Fig. 2) were performed in air up to 700 °C for 17 powdered samples from diverse lithologies. Hysteresis loops were measured for 19 samples

of selected lithologies to determine the saturation magnetization, remanent saturation and coercive force. The Curie balance measurements (Fig. 2a) show that the dominant magnetic carrier for a part of the samples is a mineral with a maximum blocking temperature (T_b) in the range of 580–620 °C, both at and slightly above the Curie temperature of magnetite (C. 580 °C) (Dunlop and Özdemir, 1997). The hysteresis curves for these samples are almost closed below 300 mT (Fig. 2b) and suggest the presence of a low coercivity mineral, most likely magnetite, possibly accompanied by a high coercivity mineral, most likely hematite. For the majority of the samples, the Curie balance measurements show invariably an increase of total magnetization after heating above 420 °C (Fig. 2c). The hysteresis loops recorded for this type of samples have a more rectangular shape (Fig. 2d), which is characteristic for (pseudo)-single domain

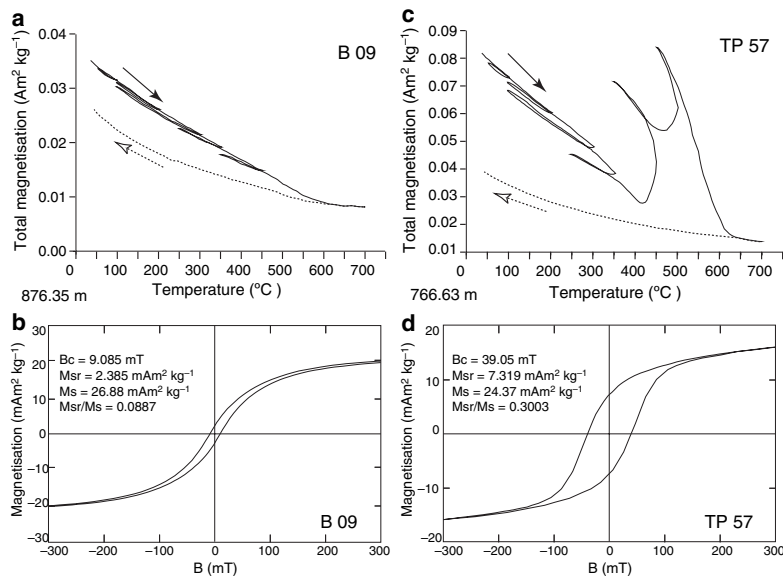


Fig. 2 Rock magnetic measurements of characteristic samples. (a) Representative thermomagnetic run for an iron oxide type of the magnetic carrier; (b) the hysteresis loop applied for the same (B 09) sample; (c) representative thermomagnetic run for a mostly iron sulphide type of the magnetic carrier; (d) the hysteresis loop applied for the same (TP 57) sample. The Curie balance measurements have been performed in air on a modified horizontal translation type Curie balance (noise level 5×10^{-9} Am²) (Mullender *et al.*, 1993). In the left-down corner is the stratigraphic level. Heating (solid line) and cooling (dashed line) were performed with rates of 10 °C min⁻¹, the cycling field varied between 150 and 300 mT. The hysteresis loops were measured for $-2T = B = 2T$, on an alternating gradient magnetometer (MicroMag Model Princeton, noise level 2×10^{-8} Am²; Princeton Measurements Corp., Princeton, NJ). In the figures, the results up to ± 300 mT are shown, and we applied paramagnetic contribution and mass corrections.

pyrrhotite (Dekkers, 1988) or greigite. The relatively high coercivity and the maximum T_b in the range 320–340° points to pyrrhotite and greigite as well.

Magnetostratigraphy

To establish the magnetostratigraphy for the Bădăslava Valley and Topolog Valley sections, at least one specimen per level was stepwise thermally demagnetized with small temperature increments of 5–30 °C up to a maximum temperature of 600 °C, in a magnetically shielded furnace. As the rock-magnetic experiments indicated the presence of iron sulphides, we chose to apply smaller heating steps between 200 and 400 °C. The directions of the NRM were calculated by principal component analysis (Kirschvink, 1980). Thermal demagnetization diagrams generally revealed a stable and well-defined characteristic remanent magnetisation (ChRM) (Fig. 3a–c), although in some cases a small secondary viscous or present-day field component was removed at temperatures below 150–180 °C. Less than 23% of the data presented a viscous type of magnetization (Fig. 3d) or a total present-day overprint and were not interpreted. In 15% of the demagnetization diagrams, most of the NRM was removed after heating at temperatures higher than 520 °C (Fig. 3a), pointing to an iron oxide type of magnetic carrier. These samples are located mostly in the older part of the Bădăslava section and record a continuous susceptibility decrease without a visible increase upon heating to the highest temperatures (600 °C). The majority of the samples (62%) record a significant increase in susceptibility and intensity after heating to temperatures of 360–420 °C, indicating the oxidation of an iron sulphide. In these diagrams, the NRM is largely removed at temperatures of approximately 390–420 °C (Fig. 3b,c). This confirms the rock magnetic conclusion that an iron sulphide is the main carrier of the remanence magnetization. Five levels in the vicinity of a polarity reversal show the antipodal magnetization of two different components (Fig. 3e,f). We believe that in these cases early diagenetic processes cause a delay in acquisition and an

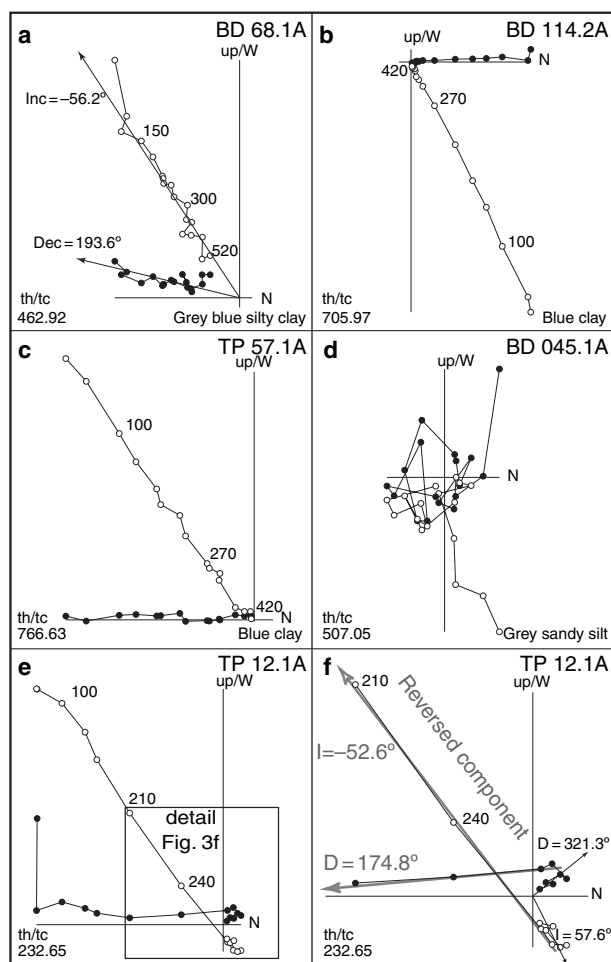


Fig. 3 Thermal demagnetization diagrams. The natural remanent magnetization (NRM) was measured on a horizontal 2G Enterprise DC SQUID cryogenic magnetometer (2G Enterprises, Pacific Grove, CA). The magnetic susceptibility was measured after each step on a Kappabridge KLY-2 (AGICO, Brno, Czech Republic) to monitor mineralogical changes. Closed (open) symbols represent the projection of the vector end points on the horizontal (vertical) plane; values represent temperature in °C; stratigraphic levels are in the lower left-hand corner; lithologies are in the right-hand corner. The diagrams are represented with tectonic correction (th/tc). The back arrows in (a) and (f) indicate the interpreted ChRM directions, D , declinations and I , inclinations; (f) illustrates one of the five cases where the ChRM (black arrows) was partly overprinted by a large reversed magnetization (grey arrows).

(partial) overprint of the original (earlier acquired) component, similar to that observed in the eastern Carpathian foredeep (Vasiliev *et al.*, 2004). Hence, the direction of the following (younger) polarity interval will overprint the original direction.

Normal and reversed components are revealed in both iron oxides and iron sulphides, suggesting a (nearly) primary origin of these magnetic components. The ChRM directions can be reliably determined from the demagnetization diagrams and reveal 11

polarity reversals in the Bădăslava section: five normal and six reversed intervals. The Topolog section recorded nine reversals with four normal and five reversed polarity intervals. The long and unambiguous polarity pattern allows an excellent correlation to the GPTS (Fig. 4).

Chronology for the South Carpathian foredeep

We used the most recent astronomically dated GPTS (Lourens *et al.*,

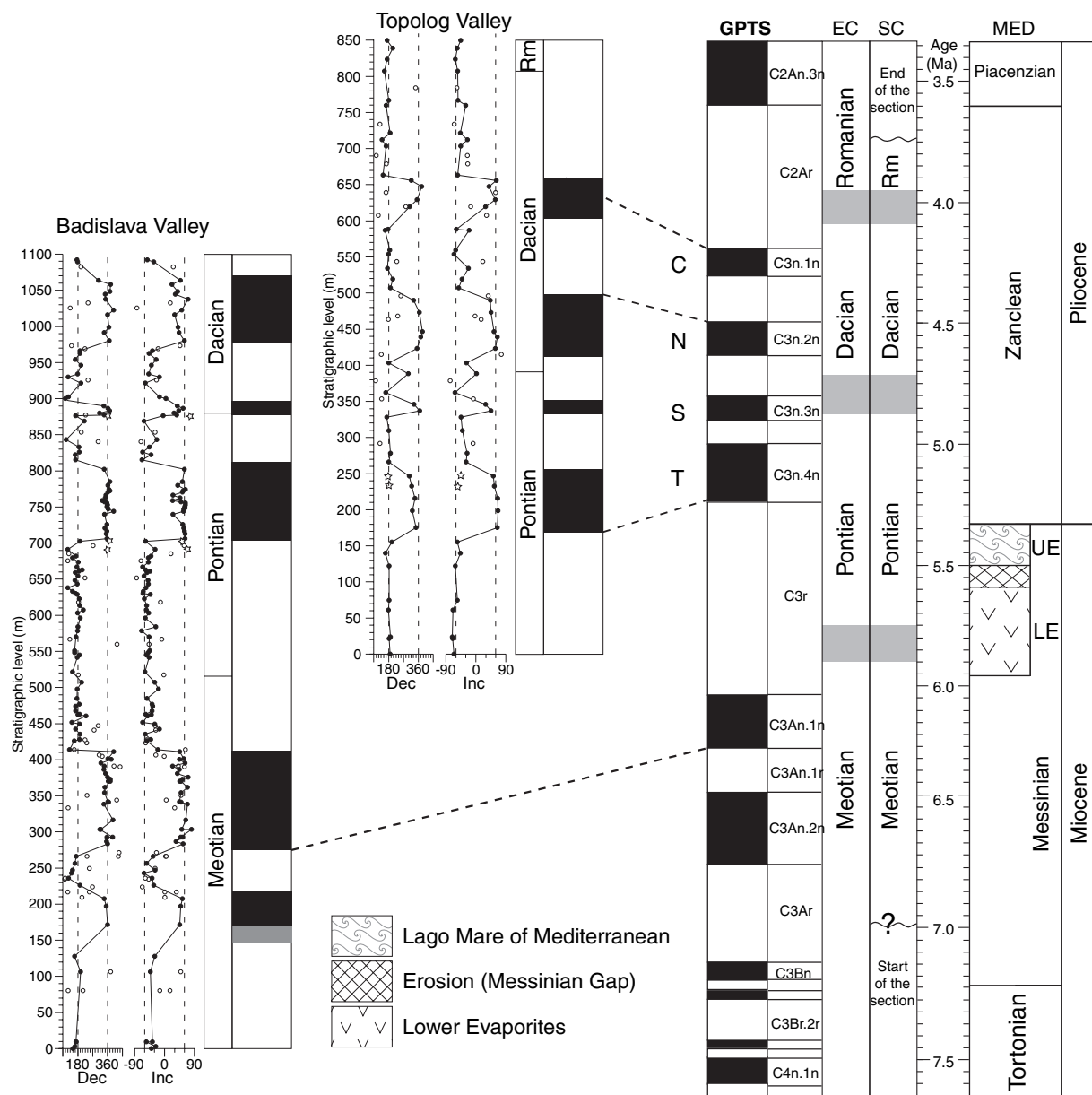


Fig. 4 Correlation of the polarity patterns of the Bădăslava and Topolog sections to the GPTS. The ages are according to (Lourens *et al.*, 2005). In the polarity columns, black and white denotes normal, respectively, reversed polarity intervals. Solid dots (●) represent reliable directions of demagnetisation diagrams. Open circles (○) represent less reliable directions contaminated or largely overprinted by present-day directions and/or viscous NRM. The white stars represent directions of low temperature components (later) magnetized in the opposite direction from the high temperature components (e.g. e and f). Next to the polarity column are the limits between different stages according to the 34 Pitești, 1 : 200 000 scale map (Bombita *et al.*, 1967). The dashed lines between the sections and GPTS connect (interpretative) simultaneous polarity boundaries. Chron nomenclature follows Cande and Kent (1992), while C (Cochiti), N (Nunivak), S (Sidufjall) and T (Thvera) are the historical names for the normal subchrons of the Gilbert Chron. The age intervals for the stage boundaries in the southern Carpathian (SC) foredeep (Bădăslava and Topolog) and the eastern Carpathians (EC) foredeep (after Vasiliev *et al.*, 2004) are approximately synchronous within uncertainty of ± 150 kyr (shaded areas). The right-hand column shows the schematic Mediterranean (MED) time scale for the Late Miocene–Early Pliocene with the Upper Messinian lower evaporites (LE) and upper evaporites (UE) units of the Messinian Salinity Crisis (after Krijgsman *et al.*, 2001).

2005) to establish the magnetostratigraphic correlation of our sections. The most striking polarity pattern in the Bădăslava and Topolog sections

(Fig. 4) is a very long reversed zone that comprises the Meotian/Pontian stage boundary from the geological map (Fig. 5). A succession of four

relatively short normal and three reversed zones is followed again by another long reversed interval. The lengths of these polarity zones are in

good agreement between the two sections and this characteristic pattern correlates excellently to subchrons C3r, C3n.4n (Thvera), C3n.3r, C3n.3n (Sidufjall), C3n.2r, C3n.2n (Nunivak), C3n.1r and C3n.1n (Cochiti), covering the time span between 6 and 3.8 Ma (Fig. 4). The most logical correlation of the two normal polarity zones in Bădislava below the long reversed interval of C3r is to C3An. The length of the lowermost normal interval, however, appears to be too short for a correlation to C3An.2n (Fig. 4). Another possible correlation of these two normal zones is to C3Bn, but this implies that a significant (~1 Myr) hiatus would be present in the lower part of the Bădislava section.

For all magnetostratigraphic sites, the GPS location has been registered with a maximum horizontal accuracy

error of 10 m. All sites were introduced on a georeferenced database and located on the geological map of the region (34 Pitești, 1:200 000 scale) (Fig. 5). From the maps, we could thus derive the magnetostratigraphic ages of the main Paratethys stage boundaries (Fig. 4). The Meotian/Pontian boundary is dated in the lower part of chron C3r at *c.* 5.8 Ma. Unfortunately, this boundary is not directly constrained by biostratigraphic data because no fossils have been observed in this part of the Bădislava and Topolog sections. The Pontian/Dacian boundary is located around C3n.3n (Sidufjall) at *c.* 4.9 Ma and the Dacian/Romanian boundary in the lower part of C2Ar, at *c.* 4.1 Ma (Figs 4 and 5). The precision of these ages depends (i) on the accuracy of the GPS measurements; (ii) on the density of the palaeomagnetic sites in the vicinity of the stage boundaries; but (iii)

most of all on the precision of the biostratigraphically determined stage boundaries.

Discussion and conclusion

Our ages from the southern Carpathian foredeep are in very good agreement with the ages obtained for the same stage boundaries in the East Carpathians (Fig. 4). This implies that the palaeoenvironmental changes inducing transformations in the faunal assemblages between different stages are synchronous (within uncertainty of *c.* 150 kyr) between the eastern and southern Carpathian foredeep. The Late Miocene and Early Pliocene stages of the eastern Paratethys are consequently at least of regional significance.

Our data from the eastern Paratethys suggests that the Meotian/Pontian boundary (*c.* 5.8 Ma) postdates the onset of Mediterranean Salinity Crisis at 5.96 Ma (Krijgsman *et al.*, 1999). This is in large contrast with previous correlations of the Meotian/Pontian boundary to the Tortonian/Messinian boundary (at *c.* 7.2 Ma) as suggested by (Rögl and Daxner-Hock, 1996). Slightly after the onset of the MSC, the marine Meotian of the Paratethys transforms to the almost freshwater environment of the Pontian Lake, probably as a result of increased river inflow or of reduction of the connections with the marine water masses. From our data, it cannot be concluded if there is a causal relation between these two events. The Lago Mare phase of the Mediterranean at 5.50–5.33 Ma took place entirely during Pontian times, but apparently has left no clear signatures in the Carpathian foredeep of Romania. We also find no (clear) evidence that the reflooding of the Mediterranean at 5.33 (Mio-Pliocene boundary) is reflected in this region. However, desiccation, reflooding and Gilbert type delta development have been reported for the Danube region (Iron Gates), where high sea-level cross-exchanges are suggested to have occurred between the Mediterranean and Central Paratethys just before and after the salinity crisis (Clauzon *et al.*, in press). The change from the Pontian freshwater environment towards the brackish-marine Dacian at 4.9 Ma does not seem to be reflected by the main

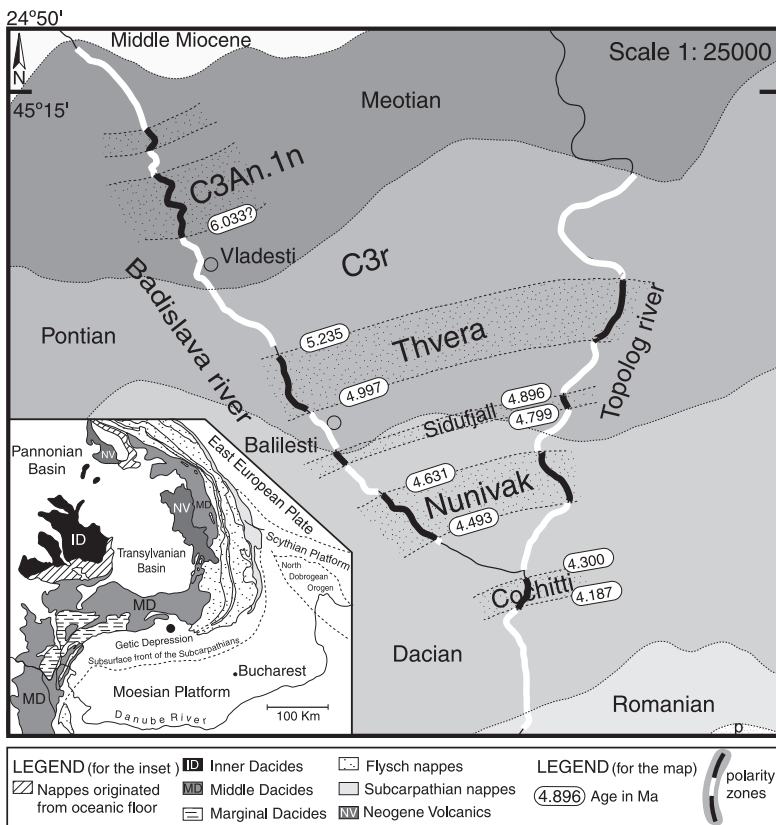


Fig. 5 Geological map of the study area (after Bombita *et al.*, 1967). The different types of shading correspond to the different Mio-Pliocene stages in the area of Bădislava and Topolog confluence. The thick white/black lines along the river trajectory show the observed reversed/normal polarity intervals. The dotted areas are the imaginary connection between two sections. In the ellipses are the magnetostratigraphic age constraints for the succession after the GPTS of Lourens *et al.* (2005). The inset represents the geological sketch of the Romanian Carpathians.

palaeoenvironmental changes in the Mediterranean. We conclude that our results show no evidence for major water exchange between the eastern Paratethys and Mediterranean domains during the late Miocene. The present-day connection through the Bosphorus opened during the late Pliocene (Görür *et al.*, 1997). Detailed biostratigraphic and isotopic records from the eastern Paratethys will be required to specify and quantify the environmental changes more precisely and to substantiate our conclusions.

Acknowledgements

This work was carried out in the frame of activities sponsored by Netherlands research Centre for Integrated Solid Earth Sciences (ISES). We thank Gabi, Guillaume, Adrian and Klaudia for their help in the field and Dr Iuliana Lazăr for providing the biostratigraphic data from her BSc thesis. We acknowledge the helpful comments of Fred Rögl and Jean Marie Rouchy.

References

- Alexeeva, L.I., Andreescu, I., Bandrabur, T., Cepaliga, A., Ghenea, C., Mihaila, N. and Trubihin, V., 1981. Correlation of the Pliocene and Lower Pleistocene deposits in the Dacic and Euxinic Basins. *Dan. Ecl. Geol. Helv.*, **8**, 143–151.
- Andreescu, I., 1981. Middle-Upper Neogene and early Quaternary chronology from the Dacic Basin and correlation with neighbouring areas. *Ann. Geol. Pays Hellen.*, tome hors serie., **4**, 129–138.
- Benammi, M., Calvo, M., Prevot, M. and Jaeger, J.-J., 1996. Magnetostratigraphy and paleontology of Ait Kandoula Basin (High Atlas, Morocco) and the African-European late Miocene terrestrial fauna exchanges. *Earth Planet. Sci. Lett.*, **145**, 15–29.
- Bombita, G., Dessila-Codarcea, M., Giurgea, P., Lupu, M., Mihaila, N. and Stancu, J., 1967. *Geologic Map of Romania, 1:200,000; Pitesti Sheet*. Geological Institute of Romania, Bucharest.
- Cande, S.C. and Kent, D.V., 1992. A new geomagnetic polarity time scale for the late Cretaceous and Cenozoic. *J. Geophys. Res.*, **97**, 13917–13951.
- Cita, M.B., Wright, R.C., Ryan, W.B.F. and Longinelli, A., 1978. Messinian paleoenvironments. Initial Reports of the Deep Sea Drilling Project. 1003–1035.
- Cita, M.B., Santambrogio, S., Mellillo, B. and Rogate, F., 1990. Messinian paleoenvironments: new evidence from the Tyrrhenian Sea (ODP Leg 107). *Sci. Results*, **107**, 211–227.
- Clauzon, G., Suc, J.-P., Popescu, S.-P., Marunteanu, M., Rubino, J.-L., Marinescu, F., Jipa, D. and Melinte, M.C., in press. Influence of the Mediterranean sea-level changes over the Dacic basin (eastern Paratethys) in the Late Neogene — The Mediterranean Lago Mare facies deciphered. *Basin Res.*, in press.
- Dekkers, M.J., 1988. *Some Rockmagnetic Parameters for Natural Goethite, Pyrrhotite and Fine-grained Hematite*. Utrecht Universiteit, Utrecht.
- Dunlop, D.J. and Özdemir, O., 1997. *Rock Magnetism – Fundamentals and Frontiers*. Cambridge University Press, Cambridge.
- Garcés, M., 2001. Chronostratigraphic framework and evolution of the Fortuna basin (Eastern Betics) since the late Miocene. *Basin Research*, **13**, 199–216.
- Garcés, M., Krijgsman, W. and Agustí, J., 1998. Chronology of the late Turolian deposits of the Fortuna basin (SE Spain): implications for the Messinian evolution of the eastern Betics. *Earth Planet. Sci. Lett.*, **163**, 69–81.
- Gautier, F., Clauzon, G., Suc, J.-P., Cravatte, J. and Violanti, D., 1994. Age et durée de la crise de salinité messinienne. *C. R. Acad. Sci. Paris*, **318**, 1103–1109.
- Görür, N., Çagatay, M.N., Sakiç, M., Sentürk, K., Yaltırak, C. and Tchapałyga, A., 1997. Origin of the Sea of Marmara as deduced from the Neogene to Quaternary Paleogeographic evolution of its frame. *Int. Geol. Rev.*, **39**, 342–352.
- Hodell, D.A., Curtis, J.H., Sierro, F.J. and Raymo, M.E., 2001. Correlation of late Miocene to early Pliocene sequences between the Mediterranean and North Atlantic. *Paleoceanography*, **16**, 164–178.
- Kirschvink, J.L., 1980. The least-squares line and plane and the analysis of paleomagnetic data. *Geophys. J. R. Astr. Soc.*, **62**, 699–718.
- Krijgsman, W., Hilgen, F.J., Raffi, I., Sierro, F.J. and Wilson, D., 1999. Chronology, causes and progression of the Messinian salinity crisis. *Nature*, **400**, 652–655.
- Krijgsman, W., Fortuin, A.R., Hilgen, F.J. and Sierro, F.J., 2001. Astrochronology for the Messinian Sorbas Basin (SE Spain) and orbital (precessional) forcing for evaporite cyclicity. *Sed. Geol.*, **140**, 43–60.
- Krijgsman, W., Gaboardi, S., Hilgen, F.J., Iaccarino, S., Kaenel, E. and Van der Laan, E., 2004. Revised astrochronology for the Ain el Beida section (Atlantic Morocco): No glacio-eustatic control for the onset of the Messinian Salinity Crisis. *Stratigraphy*, **1**, 87–101.
- Laskarev, V., 1924. *Sur le equivalents du Sarmatien superieur en Serbie: Recueil de travaux offert a M. Jovan Cvijic par ses amis et collaborateurs*, pp. 73–85.
- Lazar, I., 1987. The study of coal bearing post-Sarmatian deposits from Arges–Topolog area. Unpublished BSc thesis. University, Bucharest, Romania.
- Lourens, L.J., Hilgen, F.J., Laskar, J., Shackleton, N.J., and Wilson, D., 2005. The Neogene Period. In: *A Geologic Time Scale 2004* (F.M. Gradstein, J.G. Ogg, A.G. Smith eds). Cambridge University Press, UK.
- Mullender, T.A.T., van Velzen, A.J. and Dekkers, M.J., 1993. Continuous drift correction and separate identification of ferromagnetic and paramagnetic contribution in thermomagnetic runs. *Geophys. J. Int.*, **114**, 663–672.
- Rögl, F., 1996. Stratigraphic correlation of the Paratethys Oligocene and Miocene. *Mitt. Ges. Geol. Bergbaustud.*, **41**, 65–73.
- Rögl, F. and Daxner-Hock, G., 1996. Late Miocene Paratethys Correlation. In: *The Evolution of the Western Eurasian Neogene Mammal Faunas* (L.R. Bernor, V. Fahlbusch, H.-W. Mittmann eds), pp. 47–55. Columbia University Press, New York.
- Sandulescu, M., 1984. *Geotectonica Romaniei*. Editura Tehnica, Bucharest, 450 pp.
- Sandulescu, M., 1988. Cenozoic Tectonic History of the Carpathians. In: *The Pannonian Basin, A Study in Basin Evolution* (L.H. Royden and F. Horvath eds), *AAPG Memoir*, **28**, 17–25.
- Semenenko, V.N., 1979. Correlation of Mio-Pliocene of the Eastern Paratethys and Tethys. *Ann. Geol. Pays Hellen.*, tome hors serie, *fasc. III*, 1101–1111.
- Semenenko, V.N., 1989. Problems of the Pliocene correlation of the east Paratethys and Tethys. *Geol. Carpath., Bratislava*, **40**, 75–79.
- Steininger, F.F., Müller, C. and Rögl, F., 1988. Correlation of Central Paratethys, Eastern Paratethys, and Mediterranean Neogene Stages. In: *The Pannonian Basin, A Study in Basin Evolution* (L.H. Royden and F. Horvath eds), *AAPG Memoir*, **28**, 79–87.
- Steininger, F.F., Berggren, W.A., Kent, D.V., Bernor, R.L., Sen, S. and Agustí, J., 1996. Circum-Mediterranean Neogene (Miocene and Pliocene) Marine – Continental chronologic correlation of the European mammal units. In: *The Evolution of the Western Eurasian Neogene Mammal Faunas* (L.R. Bernor, V. Fahlbusch, H.-W. Mittmann eds), pp. 7–46. Columbia University Press, New York.
- Suc, J.P. and Bessais, E., 1990. Périennité d'un climat thermo-xérique en Sicile avant, pendant, après la crise de salinité

messiniene. *C.R. Acad. Sci. Paris*, **310**, 1701–1707.
Vasiliev, I., Krijgsman, W., Langereis, C.G., Panaiotu, C.E., Matenco, L. and Bertotti, G., 2004. Towards an astro-

chronological framework for the eastern Paratethys Mio-Pliocene sedimentary sequences of the Focsani basin (Romania). *Earth Planet. Sci. Lett.*, **227**, 231–247.

Received 16 December 2004; revised version accepted 10 March 2005